CHEMISTRY OF MATERIALS

pubs.acs.org/cm

Article

Tuning the Phase Separation by Thermal Annealing Enables High-Performance All-Small-Molecule Organic Solar Cells

Lingxian Meng,[⊥] Simin Wu,[⊥] Xiangjian Wan,* Zichao Shen, Mengyang Li, Yang Yang, Jian Wang, Guanghao Lu, Zaifei Ma, Zhaoyang Yao, Chenxi Li, and Yongsheng Chen*

Cite This: https://doi.org/10.1021/acs.chemmater.1c04293

Read Online

ACCESS | Metrics & More | Article Recommendations | Supporting Information

ABSTRACT: Tuning the phase separation within the active layer morphology is of great importance for enhancing the device performance of organic solar cells (OSCs), especially for all-small-molecule OSCs (ASM-OSCs). Herein, we demonstrate that an optimal phase separation could be achieved through thermal annealing (TA) for two small-molecule acceptors, F-2Cl- and FO-2Cl-based ASM-OSCs. The acceptor FO-2Cl, by introducing two oxygen atoms into the backbone of F-2Cl, exhibits red-shifted absorption, enhanced crystallinity, and improved electron mobility compared with F-2Cl. When using a small-molecule C8-C-F as the donor, the ASM-OSCs of F-2Cl- and FO-2Cl showed low power conversion efficiencies (PCEs) of 5.17 and 0.64%, respectively. However, with TA treatment, the PCEs of F-2Cl- and FO-2Cl-based devices were significantly improved to 12.15 and 13.91%, respectively. It was revealed that the TA treatment could effectively tune the phase separation of the active layer morphology with the interpenetrating network and contribute to the enhanced efficiency. Additionally, with TA treatment, the blend of C8-C-F:FO-2Cl demonstrated more favorable phase separation with higher crystallinity and stronger molecular packing compared with that of C8-C-F:F-2Cl. The results demonstrate that the phase separation of ASM-OSCs can be effectively tuned by TA treatment in combination with the delicate molecular design.

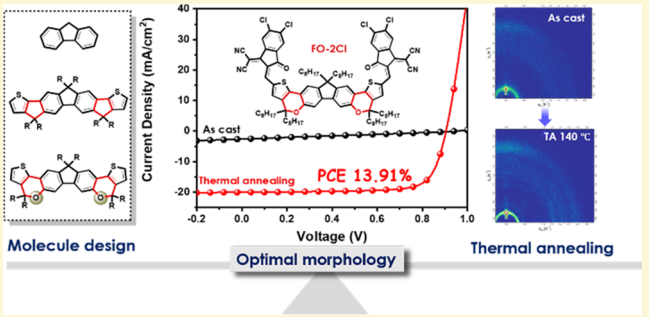

1. INTRODUCTION

As an important branch of photovoltaic technology, organic solar cells (OSCs) have drawn extensive attention with the advantages of cost-effectiveness, light weight, flexibility, and translucency.[1−6] With the 30-year continuous studies from the milestone work of Tang,[7] OSCs have experienced a dramatic development in recent years and achieved power conversion efficiencies (PCEs) over 18%.[8−14] The achievements are mainly ascribed to the design of new active layer materials, deep understanding of the device mechanism, and progress of device optimization methods[3,4,15,16] in which the active layer materials including polymers and small molecules have played a determined role to push forward the progress of the field. Compared with polymer semiconductor materials, small molecular semiconductor materials possess the merits of well-defined structures without batch-to-batch variation, easily tunable band gap, and better reproducibility.[3,4,17] Thus, all-small-molecule organic solar cells (ASM-OSCs) have drawn great attention and made great progress in the past decade.[17−20] However, photovoltaic performances of ASM-OSCs still largely lag behind their polymer-based counterpart, which could be mainly ascribed to the structural similarity of the donors and acceptors, especially for the widely used acceptor−donor−acceptor (A−D−A) type donors and acceptors, which resulted in a morphology with undesirable phase separation.[21−32] Therefore, it has become a major requisite to figure out effective ways to optimize the morphology to achieve high efficiency for ASM-OSCs. To this end, molecular-level optimizations, such as backbone and side chain engineering,[31,33] end group modulation,[34,35] *etc.*, have been used as straightforward and effective methods to manipulate the morphology. On the other hand, many strategies of device optimizations, including solvent vapor annealing (SVA),[36−38] thermal annealing (TA),[31,39] additives,[26,30] *etc.*, have been successfully used to tune the film morphology and obtain excellent device performance.[40,41] Among them, TA treatment can improve the crystallinity of the donor and acceptor, enhance the domain spacing and phase purity, and result in improved molecular ordering and optimal phase separation.[36,42] With these, it has become a widely used strategy to

Received: December 14, 2021
Revised: March 10, 2022

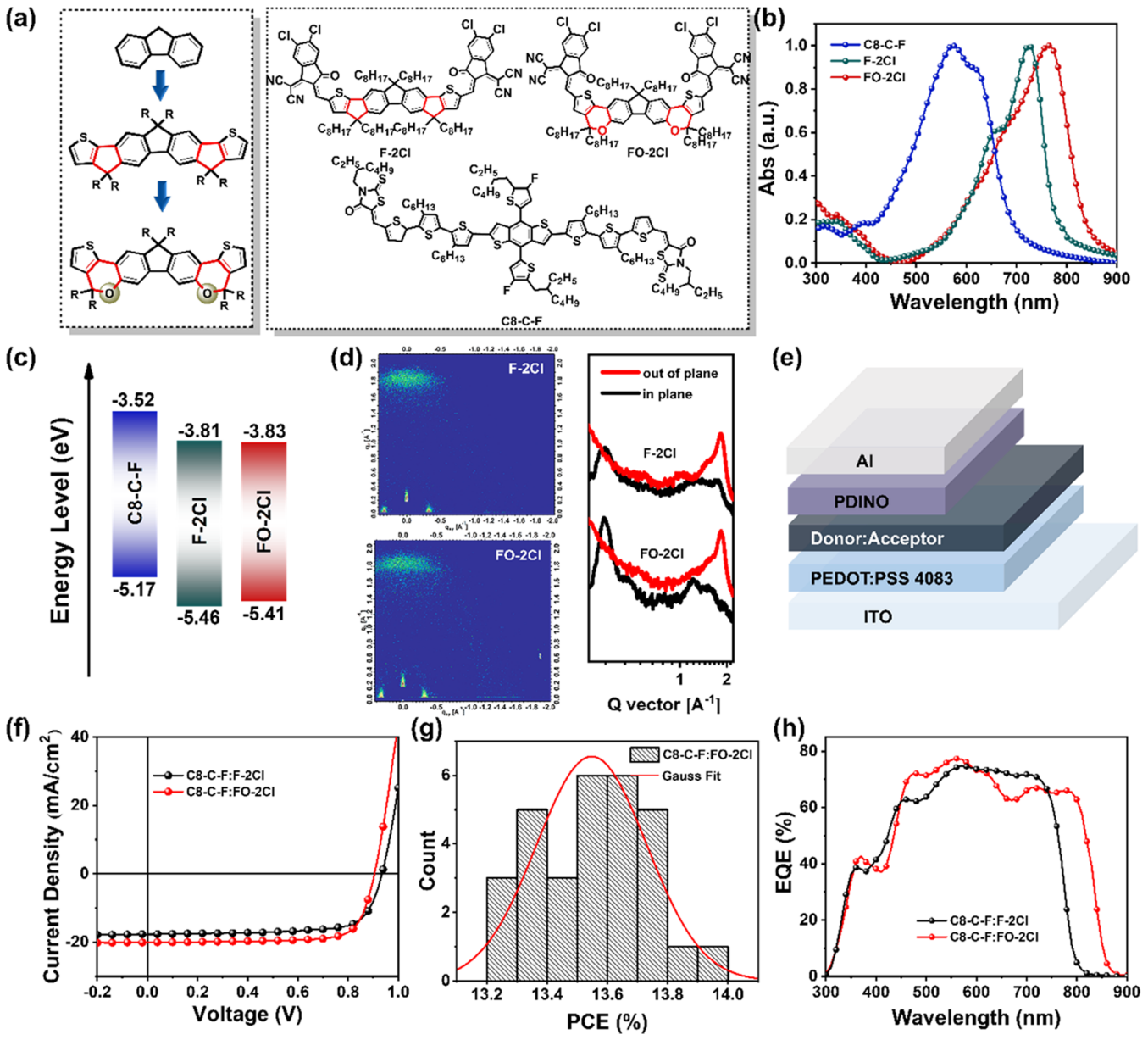

Figure 1. (a) Chemical structures of F-2Cl, FO-2Cl, and C8-C-F. (b) UV−vis absorption spectra of C8-C-F, F-2Cl, and FO-2Cl in thin films. (c) Energy levels of donor and acceptors. (d) GIWAXS and in-plane and out-of-plane line-cut profiles of neat F-2Cl and FO-2Cl films. (e) Diagram of a conventional device structure. (f) *J*−*V* curves in the optimized C8-C-F:F-2Cl/FO-2Cl-based devices. (g) Statistical diagram of PCEs for 30 individual C8-C-F:FO-2Cl-based devices with TA treatment. (h) EQE spectra in the optimized C8-C-F:F-2Cl/FO-2Cl-based devices.

optimize the active layer morphology and improve the device performance.

In recent years, we have developed a series of A−D−A type donor and acceptor materials. Among them, A−D−A type donor materials such as DR3TBDTT,[43] DRCN5T,[39] and their derivatives[3,44,45] have been widely used as small molecule donors and achieved excellent performance for ASM-OSCs. Further, we have designed a series of A−D−A type acceptors based on the similar molecular design rational of A−D−A type donors. Among them, the acceptors incorporating fluorene as the central unit have been systematically investigated by our group and some representative acceptors, such as F-M,[14,46,47] F-Br,[48,49] F-Cl,[49] and F-2Cl,[23,50] have exhibited excellent photovoltaic performances in single junction, tandem, and ternary devices.[14,48,49] Particularly, F-2Cl has been successfully used in ASM-OSCs with a wide band gap A−D−A type small-molecule donor DRTB-T and demonstrated an excellent performance.[23] But its large band gap with an absorption onset ~800 nm, which is far away from the preferred absorption with an onset (λ_{onset}) around 860−930 nm according to the semiempirical model analysis we have proposed,[3,51] is one of the intrinsic limiting factors that impacts its photovoltaic device performance. With this, in this work, we have designed and synthesized an acceptor FO-2Cl by incorporating two oxygen atoms in the backbone of F-2Cl (Figure 1a) to move down the absorption onset. Compared with F-2Cl, FO-2Cl not only has the extended absorption range but also shows an enhanced crystallinity. Two ASM-OSCs were fabricated with F-2Cl or FO-2Cl as the acceptor and an A−D−A molecule, C8-C-F, as the donor (Figure 1a). With the as-cast blend films, two ASM-OSCs of C8-C-F:F-2Cl and C8-C-F:FO-2Cl delivered low PCEs of 5.17 and 0.64%, respectively. But after

https://doi.org/10.1021/acs.chemmater.1c04293
Chem. Mater. XXXX, XXX, XXX−XXX

TA treatment, their PCEs were significantly improved to 12.15 and 13.91%, respectively. It was demonstrated that the favorable phase separation was formed in their blending films and contributed to the dramatically improved efficiencies after TA treatment. The good crystallinity and narrow band gap of FO-2Cl gave rise to its enhanced device performance compared with that of F-2Cl. The results indicate that high-performance ASM-OSCs can be realized through careful molecular design and morphology control.

2. RESULTS AND DISCUSSION

The chemical structures of F-2Cl, FO-2Cl, and C8-C-F are depicted in Figure 1a and the synthesis procedures and characterization of FO-2Cl and C8-C-F are shown in the Supporting Information. The film absorption spectra of F-2Cl and FO-2Cl, together with that of C8-C-F, are shown in Figure 1b and Table 1. Compared with F-2Cl, FO-2Cl exhibited a clearly red-shifted absorption with an onset of 848 nm and an optical band gap (E_g) of 1.46 eV, which is 0.08 eV smaller than that of F-2Cl. The energy levels of the two acceptors and the donor C8-C-F were investigated by cyclic voltammetry (Figures 1c and S1). The highest occupied molecular orbital (HOMO) level for FO-2Cl was estimated to be −5.41 eV, which is 0.05 eV higher than that of F-2Cl (−5.46 eV). With the same end groups, the lowest unoccupied molecular orbital (LUMO) level of FO-2Cl was measured to be −3.83 eV, similar to that of F-2Cl (−3.81 eV). The energy levels obtained from CV measurement are consistent with the calculated values using density functional theory at the B3LYP/6-31G* level (Figure S2). Moreover, GIWAXS measurements reveal that both the acceptors prefer face-on orientations (Figure 1d and Table S1). In comparison with F-2Cl with a $\pi-\pi$ stacking distance of 3.46 Å in the out-of-plane (OOP), FO-2Cl displays a stronger $\pi-\pi$ stacking (d = 3.44 Å). In addition, FO-2Cl shows a larger crystal coherence length (CCL) of 3.56 nm than that of F-2Cl (3.19 nm) in the (010) direction. The smaller $\pi-\pi$ stacking distance and the larger CCL of FO-2Cl indicate that the film based on FO-2Cl possesses a more ordered packing and thus higher crystallinity, which is beneficial for charge transport in the OSC devices.

To investigate the photovoltaic performance of the two NFAs, ASM-OSCs were fabricated with C8-C-F as the donor using a conventional device architecture of ITO/PEDOT:PSS/active layers/PDINO/Al, as shown in Figure 1e. After systematic device optimization (Tables S2−S6), the optimal donor and acceptor weight ratios of C8-C-F:F-2Cl and C8-C-F:FO-2Cl are all 1:0.8. The best performances of F-2Cl- and FO-2Cl-based devices were obtained via TA treatment with 120 and 140 °C for 10 min. The $J-V$ curves of the optimized devices are shown in Figure 1f. The corresponding optimized photovoltaic parameters are listed in Table 2. As shown in Table 2, with the as-cast active layer films, both the ASM-OSCs showed unfavorable performance, especially for the FO-2Cl-based device with a very low PCE of 0.64%. However, after TA treatment, the PCEs of the two ASM-OSCs were dramatically improved to 12.15 and 13.91%, respectively. Especially for the device based on FO-2Cl, its PCE was increased from 0.64% to a remarkable value of 13.91% with a high FF of 0.765 and a J_{sc} of 20.08 mA/cm^2. The histograms and corresponding Gaussian distribution of PCE counting for 30 individual C8-C-F:FO-2Cl-based devices with TA treatment are shown in Figure 1g. The impressive efficiency improvement could be attributed to the formation of the favorable morphology with proper phase separation after TA treatment on the blend film, as will be discussed below. As shown in Figure 1h, with the TA treatment, compared with the F-2Cl-based device, the FO-2Cl-based device exhibited a broader EQE response, especially in the 800−850 nm region, which results in a higher J_{sc} and could be ascribed to the red-shifted absorption of the FO-2Cl-based blend film. The integrated photocurrents of C8-C-F:F-2Cl and C8-C-F:FO-2Cl from EQE curves are 17.03 and 19.37 mA cm^{-2}, respectively, both of which are in good agreement with the J_{sc} values obtained from the corresponding $J-V$ curves.

To further evaluate the influence of the molecular design with inserting oxygen atoms on the device performances, we investigated the energy loss (E_{loss}) in both ASM-OSCs. The total E_{loss} values of F-2Cl and FO-2Cl-based devices can be obtained according to the equation $qV_{loss} = E_g - qV_{oc}$. And the total E_{loss} is usually divided into three different parts (*i.e.*, $E_{loss} = (E_g - qV_{oc,sq}) + (qV_{oc,sq} - q\Delta V_{oc,rad}) + (q\Delta V_{oc,rad} - qV_{oc}) = \Delta E_1 + \Delta E_2 + \Delta E_3$, where q is the elementary charge, V_{loss} is the voltage loss of the devices, E_g is the band gap of the blend, $V_{oc,sq}$ is the maximum voltage by the Shockley−Queisser limit where the EQE is assumed to be step-wise, $V_{oc,rad}$ is the open-circuit voltage when there is only radiative recombination, and ΔE_3 is also defined as $q\Delta V_{oc,non-rad}$, and $\Delta V_{oc,non-rad}$ is the voltage loss due to nonradiative recombination).[S2] First, the E_g of blend films is determined from the intersection of the reduced normalized absorption and PL spectra, as shown in Figure S3. Different E_g values for the two D/A systems (1.645 and 1.566 eV) indicate that solar cells based on F-2Cl and FO-2Cl have different $V_{oc,sq}$, and the corresponding energy losses (ΔE_1) (Figure 2a) of the two devices are 0.268 and 0.263 eV. Meanwhile, the device based on F-2Cl has a higher ΔE_2 of 0.187 eV compared to that of the FO-2Cl-based device (0.177 eV) (the detailed calculation is shown in Figure S4a,b and Table S7). Thus, the radiative recombination loss ($q\Delta V_{rad}$, equal to $\Delta E_1 + \Delta E_2$) of the two solar cells is identified: for the F-2Cl-based device, ΔV_{rad} is 0.455 V, but for FO-2Cl-based device, ΔV_{rad} is 0.440 V. This result indicates that the

Table 1. Optical and Electrochemical Data of C8-C-F, F-2Cl, and FO-2Cl

comp.	λ_{max}^{sol} (nm)	λ_{max}^{film} (nm)	λ_{onset} (nm)[a]	E_g (eV)[b]	HOMO (eV)	LUMO (eV)
C8-C-F	518	575	702	1.77	−5.17	−3.52
F-2Cl	690	725	805	1.54	−5.46	−3.81
FO-2Cl	708	764	848	1.46	−5.41	−3.83

[a]Absorption onset of molecular films. [b]Optical band gap was obtained from the onset wavelength of the molecular film, $E_g = 1240/\lambda_{onset}$.

Table 2. Photovoltaic Parameters of C8-C-F:F-2Cl- and C8-C-F:FO-2Cl-Based Devices under AM 1.5G Illumination (100 mW cm^{-2}) Using Conventional Device Structures

active layers	temperature (°C)	V_{oc} (V)	FF	J_{sc} (mA/cm^2)	PCE (%)[a]
C8-C-F: F-2Cl	as-cast	0.966	0.491	10.90	5.17 (4.95)
	120	0.936	0.733	17.71	12.15 (11.90)
C8-C-F: FO-2Cl	as-cast	0.952	0.257	2.61	0.64 (0.54)
	140	0.906	0.765	20.08	13.91 (13.66)

[a]The average values in parentheses are obtained from 10 independent cells.

https://doi.org/10.1021/acs.chemmater.1c04293
Chem. Mater. XXXX, XXX, XXX−XXX

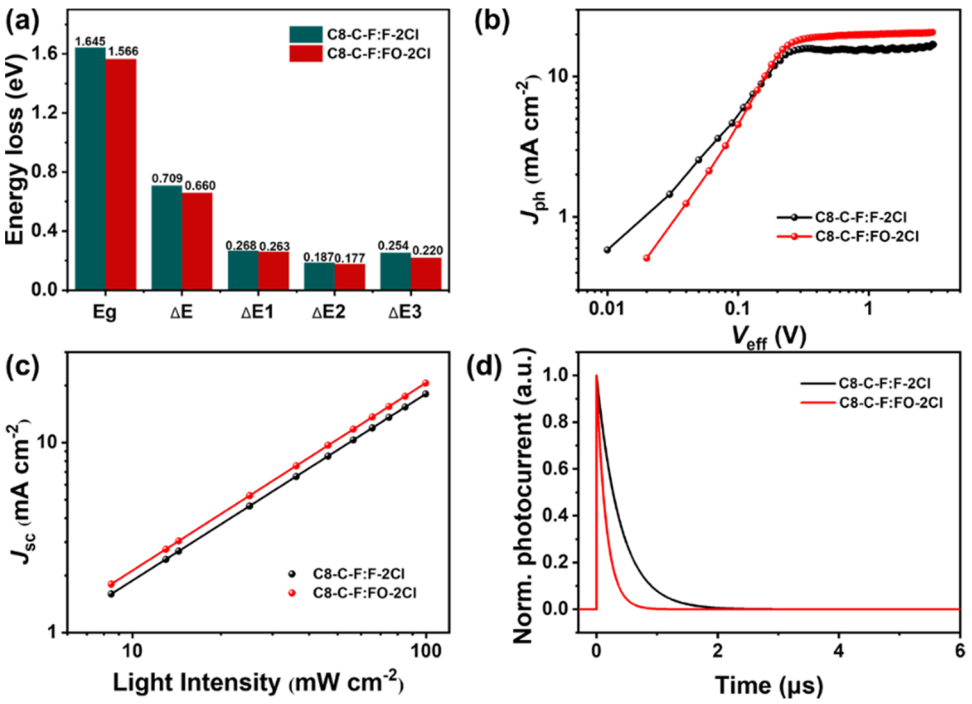

Figure 2. (a) Band gap and energy loss of the ASM-OSC devices. (b) J_{ph} versus V_{eff}, (c) light intensity (P) dependence of J_{sc}, and (d) transient photocurrent measurements of optimized C8-C-F:F-2Cl- and C8-C-F:FO-2Cl-based devices.

alteration of the molecular structure from F-2Cl to FO-2Cl has a positive effect in reducing the radiative recombination loss in OSCs. According to the above equation, the calculated ΔE_3 ($=q\Delta V_{oc,rad} - qV_{oc}$) of the two devices are 0.254 and 0.220 eV, and the device based on FO-2Cl exhibits a smaller value than that based on F-2Cl. To further confirm ΔE_3, the EQE_{EL} was also measured, and according to Figure S4c, it was found that the FO-2Cl-based device exhibits a higher EQE_{EL} (1.22×10^{-5}) than the F-2Cl-based device (6.84×10^{-6}), corresponding to the ΔV_{nr} of 0.300 and 0.286 V, and the trend of ΔV_{nr} is consistent with ΔE_3. The detailed E_{loss} values are summarized in Figure 2a and Table S7. Compared with the device of F-2Cl, the smaller E_{loss} of the FO-2Cl-based device was mainly ascribed to the smaller E_g and ΔE_3.

To study the effect of TA treatment for the charge transport properties of the two ASM-OSCs, the space charge-limited current (SCLC) method was used to study their charge transport properties. The electron and hole mobilities can be calculated by applying the Mott−Gurney law to the $J-V$ characteristics of the electron-only and hole-only devices. Although the assumptions of the Mott−Gurney law are hardly always met in organic semiconductors, such as the ohmic contacts, thickness, *etc.*,[53] the results can be compared with each other under the same measured conditions, which have been widely used in the OSC community, as shown in Figure S5 and summarized in Table S8. For the devices with the as-cast blend films, the calculated hole and electron mobilities are 1.81×10^{-4} and 0.60×10^{-4} cm^{-2} V^{-1} s^{-1} for the F-2Cl-based device and 1.41×10^{-4} and 2.14×10^{-4} cm^{-2} V^{-1} s^{-1} for the FO-2Cl-based device with mobility ratios (μ_h/μ_e) of 3.02 and 0.66, respectively. The lower and unbalanced μ_h/μ_e can be one of the reasons for the poor performance of the two ASM-OSCs, which is mainly caused by the inferior packing and unfavorable phase separation of the as-cast blend films as discussed below. After TA treatment, both the hole and electron mobilities exhibited clear enhancement with 2.04×10^{-4} (μ_h) and 1.39×10^{-4} cm^{-2} V^{-1} s^{-1} (μ_e) for the F-2Cl-based device and 2.56×10^{-4} (μ_h) and 3.29×10^{-4} cm^{-2} V^{-1} s^{-1} (μ_e) for the FO-2Cl-based device with μ_h/μ_e of 1.47 and 0.78, respectively, indicating the more ordered molecular packing in the blend films after TA treatment. The FO-2Cl-based devices clearly exhibited a higher electron mobility, indicating much better ordered packing and higher crystallinity of the molecule FO-2Cl. In addition, after TA treatment, FO-2Cl-based device showed more balanced μ_h/μ_e, which supported its much higher FF.

To further understand the charge generation and dissociation behavior in the two ASM-OSCs with TA treatment, the plot of photocurrent density (J_{ph}) versus effective voltage (V_{eff}) was measured.[54] Herein, $J_{ph} = J_L - J_D$, where J_L and J_D are the current density under illumination and in the dark, respectively, and $V_{eff} = V_0 - V_a$, where V_a is the applied voltage and V_0 is the voltage at $J_{ph} = 0$. As shown in Figure 2b, all of the devices reached saturation (J_{sat}) when the V_{eff} was ~1.5 V, indicating that the charge recombination is minimized at higher voltage. The charge dissociation probability can be estimated from the ratio of J_{ph}/J_{sat}. Under the short-circuit conditions, the J_{ph}/J_{sat} values are 91.4 and 96.6% for the F-2Cl-based and FO-2Cl-based devices, respectively, indicating the higher charge dissociation of the device based on FO-2Cl.[54,55] In addition, light intensity dependence of J_{sc} was also measured to further investigate recombination characteristics in the photoactive layers.[56] As presented in Figure 2c, the recombination parameters were obtained according to the equation $J_{sc} \propto P^{\alpha}$. The exponents were 0.98 for C8-C-F:F-2Cl and 0.99 for C8-C-F:FO-2Cl, potentially indicating that the bimolecular recombination was suppressed, especially for the FO-2Cl-based device. Figure 2d shows the transient photocurrent (TPC) decay kinetics of the F-2Cl- and FO-2Cl-based devices. The FO-2Cl-based device showed a relatively shorter sweepout time of 0.16 μs than that of F-2Cl-based device (0.39 μs). The relatively shorter charge extraction time at short-

https://doi.org/10.1021/acs.chemmater.1c04293
Chem. Mater. XXXX, XXX, XXX−XXX

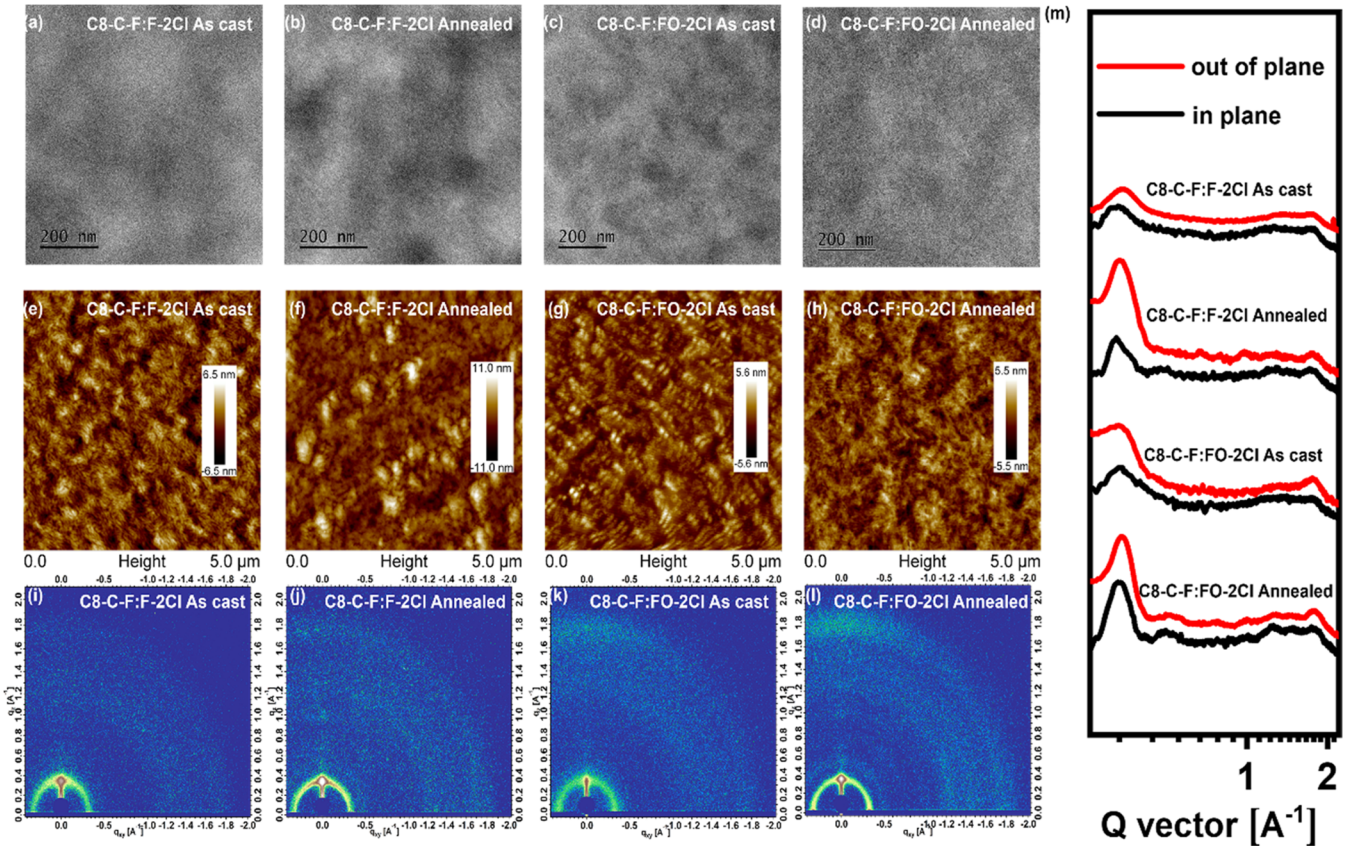

Figure 3. TEM images of C8-C-F:F-2Cl (a) as-cast and (b) annealed blend films and C8-C-F:FO-2Cl (c) as-cast and (d) annealed blend films. AFM images of C8-C-F:F-2Cl (e) as-cast and (f) annealed blend films. C8-C-F:FO-2Cl (g) as-cast and (h) annealed blend films. GIWAXS of C8-C-F:F-2Cl (i) as-cast and (j) annealed blend films. C8-C-F:FO-2Cl (k) as-cast and (l) annealed blend films. (m) In-plane and out-of-plane line cuts of the GIWAXS patterns for C8-C-F:F-2Cl and C8-C-F:FO-2Cl as-cast and annealed blend films.

circuit conditions is correlated to the observed weaker recombination in the FO-2Cl-based device. The above results demonstrated that in addition to the extended light absorption, the FO-2Cl-based device has higher efficiencies of charge transport and exciton dissociation compared with that of F-2Cl-based device.[57−59]

Transmission electron microscopy (TEM) and atomic force microscopy (AFM) measurements were taken to investigate the active layer morphologies of the two ASM-OSCs before and after TA treatment. As displayed in the TEM images of Figure 3a−d, compared with the as-cast blend films, a more clear interpenetrating network with nanoscale phase separation can be observed for the blend films after TA treatment, especially for the film of C8-C-F:FO-2Cl. From the AFM images of Figure 3e−h, the root-mean-square (RMS) roughness of the blend films of C8-C-F:F-2Cl and C8-C-F:FO-2Cl was improved from 1.63 to 2.41 and 1.24 to 1.30 nm, respectively, and the improved RMS may be related to their enhanced packing ability, indicating that TA treatment could effectively promote the exciton dissociation and charge transportation of the all-small-molecule blends.[31,60]

Grazing incidence wide-angle X-ray scattering (GIWAXS) was used to further gain insight into the molecular stacking and the influence of TA treatment. As shown in Figure S6 and Table S1, in the pristine film, the donor molecule C8-C-F shows clearly a preferential edge-on orientation with the (100) diffraction peak around 0.29 $Å^{-1}$ (d spacing: 22 Å) in the OOP direction and a $\pi-\pi$ stacking (010) diffraction around 1.69 $Å^{-1}$ (d spacing: 3.71 Å) in the in-plane (IP) direction. In contrast, the two acceptors tend to adopt face-on orientation with intense $\pi-\pi$ stacking (010) diffraction in the OOP direction as discussed above (Figure 1d). As shown in Figure 3i−m, the as-cast blend films of C8-C-F:F-2Cl and C8-C-F:FO-2Cl displayed very weak stacking behaviors both in the IP and OOP directions, which might be caused by good miscibility of the small-molecule donor and acceptor. After TA treatment, although the (100) and (010) peaks in the two blend films actually become clearer and sharper in both IP and OOP directions, their morphology changes seem rather small. In fact, owing to the similarity in the chemical structure, the morphology changes in many ASM-OSCs including our case before and after TA treatment are not as clear as those in polymer/small-molecule systems whose phases of polymer and small molecules are clearly distinct. In addition, compared with the F-2Cl-based blend film, the FO-2Cl-based blend film showed larger CCL values (3.44 and 4.74 nm for FO-2Cl and 4.01 and 3.32 nm for F-2Cl in the OOP and IP directions) and smaller $\pi-\pi$ stacking distance (3.55 and 3.58 Å for FO-2Cl and 3.60 and 3.65 Å for F-2Cl in the OOP and IP directions). The larger CCL values and smaller $\pi-\pi$ stacking distance of the FO-2Cl-based blend film demonstrated its enhanced and more ordered packing, which is beneficial for the charge transport in the OSC device.[61,62]

To further investigate the effect of TA treatment on the active layer morphologies of the two ASM-OSCs, film-depth-dependent light absorption spectra (FLAS) of the blend films without and with TA treatments on the ITO/PEDOT:PSS substrates were studied (Figure 4).[63−67] As shown in Figure 4a,

https://doi.org/10.1021/acs.chemmater.1c04293
Chem. Mater. XXXX, XXX, XXX−XXX

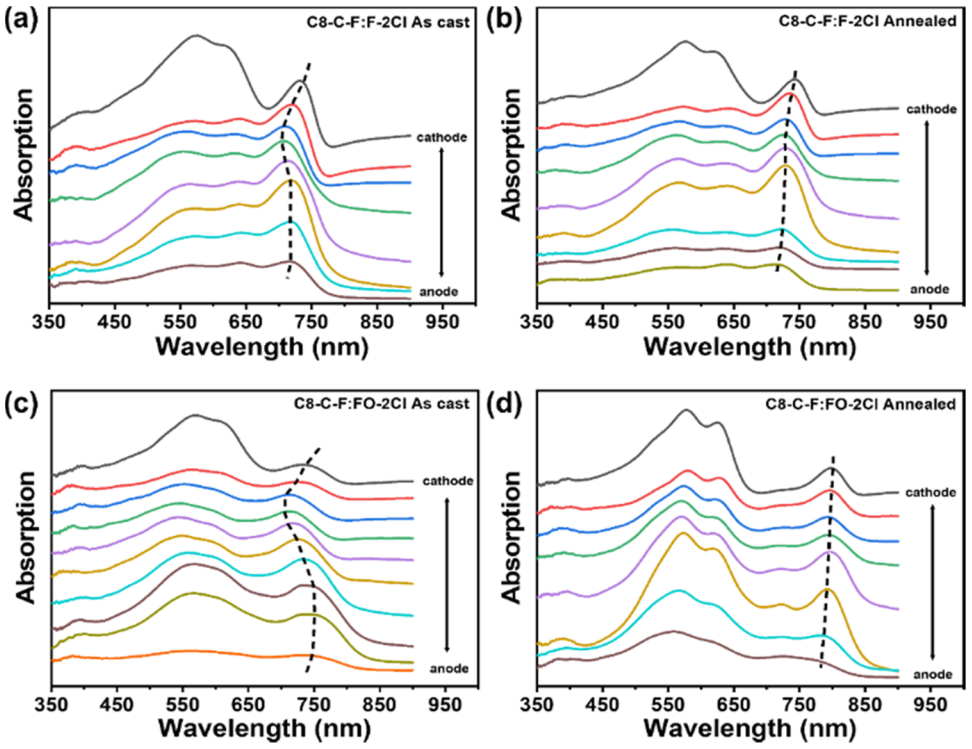

Figure 4. Film-depth-dependent absorption spectra of as-cast blend film for (a) F-2Cl-based device and (c) FO-2Cl-based device and TA blend film for (b) F-2Cl-based device and (d) FO-2Cl-based device. The dashed lines show the evolution of absorption peaks along the film-depth direction.

in the C8-C-F:F-2Cl as-cast blend film, the absorption peak around 720 nm is mainly attributed to the acceptor F-2Cl, while the absorption from 500 to 680 nm is mainly derived from the donor C8-C-F. Upon TA treatment (Figure 4b), the blend film presented red-shifted absorption resulting from the stronger molecular ordering of both donor and acceptor molecules. In addition, for C8-C-F, the peak at 568 nm and the shoulder peak at 631 nm become intense and sharp, indicating an enhancement in the crystallinity of the corresponding films caused by TA treatment. In contrast, a more complicated case of the FO-2Cl-based blend film was observed as shown in Figure 4c,d. For the FO-2Cl-based as-cast blend film, the absorption of C8-C-F in the range of 500−680 nm indicated an inferior packing of the donor. Meanwhile, the maximum absorption peak of FO-2Cl was blue-shifted to 726 nm compared to its pure film with a maximum absorption peak at 764 nm, which might be caused by worse packing and phase separation of the donor and acceptor in the as-cast blend film. The worse packing of the FO-2Cl-based as-cast blend film led to the low device efficiency with a value of only 0.64%. However, after TA treatment, a new peak at 793 nm appeared due to the higher molecular ordering of FO-2Cl. Moreover, the peak of the donor also becomes intense and sharp. These results demonstrated that TA treatment could improve the molecular packing and tune the phase separation of the blend film, which is consistent with the results from TEM, AFM, GIWASX, and SCLC.

In addition, the FLAS measurement can provide the information of the film-depth-dependent electronic properties, *i.e.*, HOMO/LUMO levels and their vertical distribution manifesting the energetic disorder of localized state dependences on the position of the film and reflecting the phase separation of the film morphology.[64−66] Before reaching the electrodes, the hole/electrons hop among localized states and the energies are directly correlated with the HOMO/LUMO levels. In some systems, because of the improper vertical phase separation, HOMO/LUMO levels could have tremendous fluctuations along the film-depth direction. This could thus lead to low-energy localized states within the film and even charge traps, resulting in inferior V_{oc} and FF. In this work, poor crystalline ordering was observed in the two blend films without TA treatment, especially for the blend film of FO-2Cl. Furthermore, their crystallinities are also dispersive along the film-depth direction, as shown by vertical fluctuation of absorption peaks (dashed lines in Figure 4a,c), corresponding to substantial dispersion of transport levels and poor photovoltaic performance. Fortunately, TA treatment changed the situation. As can be seen from the TA-treated active layers, the absorption peaks do not vary apparently along the film-depth direction, implying that the electronic transport levels have weak film-depth fluctuation and are beneficial for avoiding low-energy localized states and traps. The above results suggested that the proper phase separation with the higher molecular ordering was formed for the two ASM-OSCs after TA treatment.

3. CONCLUSIONS

In summary, we have designed and synthesized a new A−D−A type acceptor FO-2Cl by inserting two oxygen atoms in the molecular backbone of acceptor F-2Cl. Compared with F-2Cl, FO-2Cl showed red-shifted absorption and high crystallinity. With TA treatment, the PCE of C8-C-F:FO-2Cl-based ASM-OSC was improved dramatically from the value of 0.64 to 13.91%. It was found that the TA treatment could effectively manipulate the film morphology with suitable phase separation, rendering a better interpenetrating network.

https://doi.org/10.1021/acs.chemmater.1c04293
Chem. Mater. XXXX, XXX, XXX−XXX

Thus, the efficiencies of charge dissociation and transport could be enhanced and high photovoltaic device performance was achieved. The results highlight the importance of the new active layer material design as well as the device optimization strategy. It is believed that high efficiency ASM-OSCs can be realized through the combination of careful molecular design and morphology control.

4. EXPERIMENTAL SECTION

4.1. Materials and Synthesis. The details for the synthesis of FO-2Cl and C8-C-F are described in the Supporting Information. All of the corresponding NMR and MS spectra of the molecules are shown in Figures S7−S14.

4.2. Fabrication of OSCs. The devices were fabricated with an architecture of glass/ITO/PEDOT:PSS/active layers/PDINO/Al. The ITO-coated glass substrates were cleaned by ultrasonic treatment in the detergent, deionized water, acetone, and isopropyl alcohol under ultrasonication for 15 min each and subsequently dried using a nitrogen blower. A thin layer (~20 nm) of PEDOT:PSS (Clevios P VP AI 4083, filtered at 0.45 μm) was spin-coated at 4000 rpm onto the ITO surface. After baking at 150 °C for 20 min, the substrates were transferred into an argon-filled glovebox. Subsequently, the blend solution of C8-C-F:F-2Cl or C8-C-F:FO-2Cl (1:0.8 w/w, 8 mg/mL from CF) was spin-coated to form the active layers with a thickness of 120 nm. Then, the substrates were thermally treated at 120°C for C8-C-F:F-2Cl and 140 °C for C8-C-F:FO-2Cl. After that, the methanol solution of PDINO (1 mg/mL) was spin-coated on the top of active layers at 3000 rpm. Finally, 50 nm Al layers were deposited under high vacuum ($<1.5 \times 10^{-4}$ Pa). The effective areas of cells were 4 mm^2, defined by shallow masks.

4.3. Characterization of Films and Devices. The current density−voltage (J−V) curves of photovoltaic devices were obtained by a Keithley 2400 source-measure unit. The photocurrent was measured under AM 1.5G illumination at 100 mW cm^{-2} irradiation using a SAN-EI XES-70S1 solar simulator, calibrated with a standard Si solar cell. The external quantum efficiency (EQE) spectrum was measured using a QE-R Solar Cell Spectral Response Measurement System (Enli Technology Co., Ltd., Taiwan).

■ ASSOCIATED CONTENT

Supporting Information

The Supporting Information is available free of charge at https://pubs.acs.org/doi/10.1021/acs.chemmater.1c04293.

Synthetic route of the molecules, DFT calculations, CV, UV−vis, SCLC, GIWAXS patterns, and additional tables (PDF)

■ AUTHOR INFORMATION

Corresponding Authors

Xiangjian Wan − *State Key Laboratory of Elemento-Organic Chemistry. The Centre of Nanoscale Science and Technology and Key Laboratory of Functional Polymer Materials, Institute of Polymer Chemistry, College of Chemistry. Renewable Energy Conversion and Storage Center (RECAST), Nankai University, Tianjin 300071, China;* orcid.org/0000-0001-5266-8510; Email: xjwan@nankai.edu.cn

Yongsheng Chen − *State Key Laboratory of Elemento-Organic Chemistry. The Centre of Nanoscale Science and Technology and Key Laboratory of Functional Polymer Materials, Institute of Polymer Chemistry, College of Chemistry. Renewable Energy Conversion and Storage Center (RECAST), Nankai University, Tianjin 300071, China;* orcid.org/0000-0003-1448-8177; Email: yschen99@nankai.edu.cn

Authors

Lingxian Meng − *State Key Laboratory of Elemento-Organic Chemistry. The Centre of Nanoscale Science and Technology and Key Laboratory of Functional Polymer Materials, Institute of Polymer Chemistry, College of Chemistry. Renewable Energy Conversion and Storage Center (RECAST), Nankai University, Tianjin 300071, China*

Simin Wu − *State Key Laboratory of Elemento-Organic Chemistry. The Centre of Nanoscale Science and Technology and Key Laboratory of Functional Polymer Materials, Institute of Polymer Chemistry, College of Chemistry. Renewable Energy Conversion and Storage Center (RECAST), Nankai University, Tianjin 300071, China*

Zichao Shen − *Frontier Institute of Science and Technology, Xi'an Jiaotong University, Xi'an 710054, China*

Mengyang Li − *Center for Advanced Low-dimension Materials, State Key Laboratory for Modification of Chemical Fibers and Polymer Materials, College of Materials Science and Engineering, Donghua University, Shanghai 201620, China*

Yang Yang − *The Institute of Seawater Desalination and Multipurpose Utilization, Ministry of Natural Resources (Tianjin), Tianjin 300192, China*

Jian Wang − *The Institute of Seawater Desalination and Multipurpose Utilization, Ministry of Natural Resources (Tianjin), Tianjin 300192, China*

Guanghao Lu − *Frontier Institute of Science and Technology, Xi'an Jiaotong University, Xi'an 710054, China*

Zaifei Ma − *Center for Advanced Low-dimension Materials, State Key Laboratory for Modification of Chemical Fibers and Polymer Materials, College of Materials Science and Engineering, Donghua University, Shanghai 201620, China;* orcid.org/0000-0002-3100-1570

Zhaoyang Yao − *State Key Laboratory of Elemento-Organic Chemistry. The Centre of Nanoscale Science and Technology and Key Laboratory of Functional Polymer Materials, Institute of Polymer Chemistry, College of Chemistry. Renewable Energy Conversion and Storage Center (RECAST), Nankai University, Tianjin 300071, China;* orcid.org/0000-0003-1384-183X

Chenxi Li − *State Key Laboratory of Elemento-Organic Chemistry. The Centre of Nanoscale Science and Technology and Key Laboratory of Functional Polymer Materials, Institute of Polymer Chemistry, College of Chemistry. Renewable Energy Conversion and Storage Center (RECAST), Nankai University, Tianjin 300071, China*

Complete contact information is available at: https://pubs.acs.org/10.1021/acs.chemmater.1c04293

Author Contributions

⊥L.M. and S.W. contributed equally to this work.

Notes

The authors declare no competing financial interest.

■ ACKNOWLEDGMENTS

The authors gratefully acknowledge the financial support from NSFC (52025033, 21935007, and 51873089), MoST (2019YFA0705900) of China, Tianjin city (20JCZDJC00740), and the 111 Project (B12015).

REFERENCES

(1) Kim, J. Y.; Lee, K.; Coates, N. E.; Moses, D.; Nguyen, T.-Q.; Dante, M.; Heeger, A. J. Efficient Tandem Polymer Solar Cells Fabricated by All-Solution Processing. *Science* **2007**, *317*, 222−225.

(2) Sun, R.; Wu, Q.; Guo, J.; Wang, T.; Wu, Y.; Qiu, B. B.; Luo, Z. H.; Yang, W. Y.; Hu, Z. C.; Guo, J.; Shi, M. M.; Yang, C. L.; Huang, F.; Li, Y. F.; Min, J. A Layer-by-Layer Architecture for Printable Organic Solar Cells Overcoming the Scaling Lag of Module Efficiency. *Joule* **2020**, *4*, 407−419.

(3) Wan, X.; Li, C.; Zhang, M.; Chen, Y. Acceptor-Donor-Acceptor Type Molecules for High Performance Organic Photovoltaics - Chemistry and Mechanism. *Chem. Soc. Rev.* **2020**, *49*, 2828−2842.

(4) Hou, J.; Inganas, O.; Friend, R. H.; Gao, F. Organic Solar Cells Based on Non-Fullerene Acceptors. *Nat. Mater.* **2018**, *17*, 119−128.

(5) Sun, Y.; Chang, M.; Meng, L.; Wan, X.; Gao, H.; Zhang, Y.; Zhao, K.; Sun, Z.; Li, C.; Liu, S.; Wang, H.; Liang, J.; Chen, Y. Flexible Organic Photovoltaics based on Water-Processed Silver Nanowire Electrodes. *Nat. Electron.* **2019**, *2*, 513−520.

(6) Chen, X.; Xu, G.; Zeng, G.; Gu, H.; Chen, H.; Xu, H.; Yao, H.; Li, Y.; Hou, J.; Li, Y. Realizing Ultrahigh Mechanical Flexibility and>15% Efficiency of Flexible Organic Solar Cells via a "Welding" Flexible Transparent Electrode. *Adv. Mater.* **2020**, *32*, No. 1908478.

(7) Tang, C. W. Two-Layer Organic Photovoltaic Cell. *Appl. Phys. Lett.* **1986**, *48*, 183−185.

(8) Liu, Q.; Jiang, Y.; Jin, K.; Qin, J.; Xu, J.; Li, W.; Xiong, J.; Liu, J.; Xiao, Z.; Sun, K.; Yang, S.; Zhang, X.; Ding, L. 18% Efficiency Organic Solar Cells. *Sci. Bull.* **2020**, *65*, 272−275.

(9) Yao, J.; Qiu, B.; Zhang, Z. G.; Xue, L.; Wang, R.; Zhang, C.; Chen, S.; Zhou, Q.; Sun, C.; Yang, C.; Xiao, M.; Meng, L.; Li, Y. Cathode Engineering with Perylene-Diimide Interlayer Enabling over 17% Efficiency Single-Junction Organic Solar Cells. *Nat. Commun.* **2020**, *11*, No. 2726.

(10) Cui, Y.; Yao, H.; Zhang, J.; Xian, K.; Zhang, T.; Hong, L.; Wang, Y.; Xu, Y.; Ma, K.; An, C.; He, C.; Wei, Z.; Gao, F.; Hou, J. Single-Junction Organic Photovoltaic Cells with Approaching 18% Efficiency. *Adv. Mater.* **2020**, *32*, No. 1908205.

(11) Zhu, L.; Zhang, M.; Zhou, G.; Hao, T.; Xu, J.; Wang, J.; Qiu, C.; Prine, N.; Ali, J.; Feng, W.; Gu, X.; Ma, Z.; Tang, Z.; Zhu, H.; Ying, L.; Zhang, Y.; Liu, F. Efficient Organic Solar Cell with 16.88% Efficiency Enabled by Refined Acceptor Crystallization and Morphology with Improved Charge Transfer and Transport Properties. *Adv. Energy Mater.* **2020**, *10*, No. 1904234.

(12) Li, Q.; Wang, L.-M.; Liu, S.; Guo, L.; Dong, S.; Ma, G.; Cao, Z.; Zhan, X.; Gu, X.; Zhu, T.; Cai, Y.-P.; Huang, F. Vertical Composition Distribution and Crystallinity Regulations Enable High-Performance Polymer Solar Cells with>17% Efficiency. *ACS Energy Lett.* **2020**, *5*, 3637−3646.

(13) Zhan, L.; Li, S.; Lau, T.-K.; Cui, Y.; Lu, X.; Shi, M.; Li, C.-Z.; Li, H.; Hou, J.; Chen, H. Over 17% Efficiency Ternary Organic Solar Cells Enabled by Two Non-Fullerene Acceptors Working in an Alloy-like Model. *Energy Environ. Sci.* **2020**, *13*, 635−645.

(14) Meng, L.; Zhang, Y.; Wan, X.; Li, C.; Zhang, X.; Wang, Y.; Ke, X.; Xiao, Z.; Ding, L.; Xia, R.; Yip, H.-L.; Cao, Y.; Chen, Y. Organic and Solution-Processed Tandem Solar Cells with 17.3% Efficiency. *Science* **2018**, *361*, 1094−1098.

(15) Yuan, J.; Zhang, Y.; Zhou, L.; Zhang, G.; Yip, H.-L.; Lau, T.-K.; Lu, X.; Zhu, C.; Peng, H.; Johnson, P. A.; Leclerc, M.; Cao, Y.; Ulanski, J.; Li, Y.; Zou, Y. Single-Junction Organic Solar Cell with over 15% Efficiency Using Fused-Ring Acceptor with Electron-Deficient Core. *Joule* **2019**, *3*, 1140−1151.

(16) Zhang, G.; Zhao, J.; Chow, P. C. Y.; Jiang, K.; Zhang, J.; Zhu, Z.; Zhang, J.; Huang, F.; Yan, H. Nonfullerene Acceptor Molecules for Bulk Heterojunction Organic Solar Cells. *Chem. Rev.* **2018**, *118*, 3447−3507.

(17) Chen, Y.; Wan, X.; Long, G. High Performance Photovoltaic Applications Using Solution-Processed Small Molecules. *Acc. Chem. Res.* **2013**, *46*, 2645−2655.

(18) Huo, Y.; Zhang, H.-L.; Zhan, X. Nonfullerene All-Small-Molecule Organic Solar Cells. *ACS Energy Lett.* **2019**, *4*, 1241−1250.

(19) Ye, W.; Yang, Y.; Zhang, Z.; Zhu, Y.; Ye, L.; Miao, C.; Lin, Y.; Zhang, S. Nonfullerene All-Small-Molecule Organic Solar Cells: Prospect and Limitation. *Sol. RRL* **2020**, *4*, No. 2000258.

(20) Qin, J.; Chen, Z.; Bi, P.; Yang, Y.; Zhang, J.; Huang, Z.; Wei, Z.; An, C.; Yao, H.; Hao, X.; Zhang, T.; Cui, Y.; Hong, L.; Liu, C.; Zu, Y.; He, C.; Hou, J. 17% Efficiency in All-Small-Molecule Organic Solar Cells Enabled by Nanoscale Phase Separation with Hierarchical Branched Structure. *Energy Environ. Sci.* **2021**, *14*, 5903−5910.

(21) Bin, H.; Yang, Y.; Zhang, Z.-G.; Ye, L.; Ghasem, M.; Chen, S.; Zhang, Y.; Zhang, C.; Sun, C.; Xue, L.; Yang, C.; Ade, H.; Li, Y. 9.73% Efficiency Nonfullerene All Organic Small Molecule Solar Cells with Absorption-Complementary Donor and Acceptor. *J. Am. Chem. Soc.* **2017**, *139*, 5085−5094.

(22) Yang, L.; Zhang, S.; He, C.; Zhang, J.; Yao, H.; Yang, Y.; Zhang, Y.; Zhao, W.; Hou, J. New Wide Band Gap Donor for Efficient Fullerene-Free All-Small-Molecule Organic Solar Cells. *J. Am. Chem. Soc.* **2017**, *139*, 1958−1966.

(23) Wang, Y.; Wang, Y.; Kan, B.; Ke, X.; Wan, X.; Li, C.; Chen, Y. High-Performance All-Small-Molecule Solar Cells Based on a New Type of Small Molecule Acceptors with Chlorinated End Groups. *Adv. Energy Mater.* **2018**, *8*, No. 1802021.

(24) Zhou, Z.; Xu, S.; Song, J.; Jin, Y.; Yue, Q.; Qian, Y.; Liu, F.; Zhang, F.; Zhu, X. High-Efficiency Small-Molecule Ternary Solar Cells with a Hierarchical Morphology Enabled by Synergizing Fullerene and Non-Fullerene Acceptors. *Nat. Energy* **2018**, *3*, 952−959.

(25) Chen, H.; Hu, D.; Yang, Q.; Gao, J.; Fu, J.; Yang, K.; He, H.; Chen, S.; Kan, Z.; Duan, T.; Yang, C.; Ouyang, J.; Xiao, Z.; Sun, K.; Lu, S. All-Small-Molecule Organic Solar Cells with an Ordered Liquid Crystalline Donor. *Joule* **2019**, *3*, 3034−3047.

(26) Gao, K.; Jo, S. B.; Shi, X.; Nian, L.; Zhang, M.; Kan, Y.; Lin, F.; Kan, B.; Xu, B.; Rong, Q.; Shui, L.; Liu, F.; Peng, X.; Zhou, G.; Cao, Y.; Jen, A. K. Over 12% Efficiency Nonfullerene All-Small-Molecule Organic Solar Cells with Sequentially Evolved Multilength Scale Morphologies. *Adv. Mater.* **2019**, *31*, No. 1807842.

(27) Ge, J.; Xie, L.; Peng, R.; Fanady, B.; Huang, J.; Song, W.; Yan, T.; Zhang, W.; Ge, Z. 13.34% Efficiency Non-Fullerene All-Small-Molecule Organic Solar Cells Enabled by Modulating the Crystallinity of Donors via a Fluorination Strategy. *Angew. Chem., Int. Ed.* **2020**, *59*, 2808−2815.

(28) Zhou, R.; Jiang, Z.; Yang, C.; Yu, J.; Feng, J.; Adil, M. A.; Deng, D.; Zou, W.; Zhang, J.; Lu, K.; Ma, W.; Gao, F.; Wei, Z. All-Small-Molecule Organic Solar Cells with over 14% Efficiency by Optimizing Hierarchical Morphologies. *Nat. Commun.* **2019**, *10*, No. 5393.

(29) Hu, D.; Yang, Q.; Chen, H.; Wobben, F.; Le Corre, V. M.; Singh, R.; Liu, T.; Ma, R.; Tang, H.; Koster, L. J. A.; Duan, T.; Yan, H.; Kan, Z.; Xiao, Z.; Lu, S. 15.34% Efficiency All-Small-Molecule Organic Solar Cells with Improved Fill Factor Enabled by A Fullerene Additive. *Energy Environ. Sci.* **2020**, *13*, 2134−2141.

(30) Nian, L.; Kan, Y.; Gao, K.; Zhang, M.; Li, N.; Zhou, G.; Jo, S. B.; Shi, X.; Lin, F.; Rong, Q.; Feng, Liu.; Zhou, G.; Jen, A. K.-Y. Approaching 16% Efficiency in All-SmallMolecule Organic Solar Cells Based on Ternary Strategy with a Highly Crystalline Acceptor. *Joule* **2020**, *4*, 2223−2236.

(31) Qiu, B.; Chen, Z.; Qin, S.; Yao, J.; Huang, W.; Meng, L.; Zhu, H.; Yang, Y. M.; Zhang, Z. G.; Li, Y. Highly Efficient All-Small-Molecule Organic Solar Cells with Appropriate Active Layer Morphology by Side Chain Engineering of Donor Molecules and Thermal Annealing. *Adv. Mater.* **2020**, *32*, No. 1908373.

(32) Wang, Y.; Wang, Y.; Zhu, L.; Liu, H.; Fang, J.; Guo, X.; Liu, F.; Tang, Z.; Zhang, M.; Li, Y. A Novel Wide-Bandgap Small Molecule Donor for High Efficiency All-Small-Molecule Organic Solar Cells with Small Non-Radiative Energy Losses. *Energy Environ. Sci.* **2020**, *13*, 1309−1317.

(33) Gao, J.; Ge, J.; Peng, R.; Liu, C.; Cao, L.; Zhang, D.; Fanady, B.; Hong, L.; Zhou, E.; Ge, Z. Over 14% Efficiency Nonfullerene All-Small-Molecule Organic Solar Cells Enabled by Improving the Ordering of Molecular Donors via Side-Chain Engineering. *J. Mater. Chem. A* **2020**, *8*, 7405−7411.

https://doi.org/10.1021/acs.chemmater.1c04293
Chem. Mater. XXXX, XXX, XXX−XXX

(34) Wu, Q.; Deng, D.; Zhou, R.; Zhang, J.; Zou, W.; Liu, L.; Wu, S.; Lu, K.; Wei, Z. Modulation of Donor Alkyl Terminal Chains with the Shifting Branching Point Leads to the Optimized Morphology and Efficient All-Small-Molecule Organic Solar Cells. *ACS Appl. Mater. Interfaces* **2020**, *12*, 25100−25107.
(35) Yang, L.; Zhang, S.; He, C.; Zhang, J.; Yang, Y.; Zhu, J.; Cui, Y.; Zhao, W.; Zhang, H.; Zhang, Y.; Wei, Z.; Hou, J. Modulating Molecular Orientation Enables Efficient Nonfullerene Small-Molecule Organic Solar Cells. *Chem. Mater.* **2018**, *30*, 2129−2134.
(36) Min, J.; Güldal, N. S.; Guo, J.; Fang, C.; Jiao, X.; Hu, H.; Heumüller, T.; Ade, H.; Brabec, C. J. Gaining Further Insight into the Effects of Thermal Annealing and Solvent Vapor Annealing on Time Morphological Development and Degradation in Small Molecule Solar Cells. *J. Mater. Chem. A* **2017**, *5*, 18101−18110.
(37) Li, M.; Liu, F.; Wan, X.; Ni, W.; Kan, B.; Feng, H.; Zhang, Q.; Yang, X.; Wang, Y.; Zhang, Y.; Shen, Y.; Russell, T. P.; Chen, Y. Subtle Balance Between Length Scale of Phase Separation and Domain Purification in Small-Molecule Bulk-Heterojunction Blends under Solvent Vapor Treatment. *Adv. Mater.* **2015**, *27*, 6296−6302.
(38) Min, J.; Jiao, X.; Ata, I.; Osvet, A.; Ameri, T.; Bäuerle, P.; Ade, H.; Brabec, C. J. Time-Dependent Morphology Evolution of Solution-Processed Small Molecule Solar Cells during Solvent Vapor Annealing. *Adv. Energy Mater.* **2016**, *6*, No. 1502579.
(39) Kan, B.; Li, M.; Zhang, Q.; Liu, F.; Wan, X.; Wang, Y.; Ni, W.; Long, G.; Yang, X.; Feng, H.; Zuo, Y.; Zhang, M.; Huang, F.; Cao, Y.; Russell, T. P.; Chen, Y. A Series of Simple Oligomer-like Small Molecules Based on Oligothiophenes for Solution-Processed Solar Cells with High Efficiency. *J. Am. Chem. Soc.* **2015**, *137*, 3886−3893.
(40) Wang, Y.; Lee, J.; Hou, X.; Labanti, C.; Yan, J.; Mazzolini, E.; Parhar, A.; Nelson, J.; Kim, J. S.; Li, Z. Recent Progress and Challenges toward Highly Stable Nonfullerene Acceptor-Based Organic Solar Cells. *Adv. Energy Mater.* **2021**, *11*, No. 2003002.
(41) McDowell, C.; Abdelsamie, M.; Toney, M. F.; Bazan, G. C. Solvent Additives: Key Morphology-Directing Agents for Solution-Processed Organic Solar Cells. *Adv. Mater.* **2018**, *30*, No. 1707114.
(42) Guo, J.; Bin, H.; Wang, W.; Chen, B.; Guo, J.; Sun, R.; Zhang, Z.-G.; Jiao, X.; Li, Y.; Min, J. All-Small Molecule Solar Cells based on Donor Molecule Optimization with Highly Enhanced Efficiency and Stability. *J. Mater. Chem. A* **2018**, *6*, 15675−15683.
(43) Zhou, J.; Zuo, Y.; Wan, X.; Long, G.; Zhang, Q.; Ni, W.; Liu, Y.; Li, Z.; He, G.; Li, C.; Kan, B.; Li, M.; Chen, Y. Solution-Processed and High-Performance Organic Solar Cells Using Small Molecules with a Benzodithiophene Unit. *J. Am. Chem. Soc.* **2013**, *135*, 8484−8487.
(44) Zhang, Q.; Kan, B.; Liu, F.; Long, G.; Wan, X.; Chen, X.; Zuo, Y.; Ni, W.; Zhang, H.; Li, M.; Hu, Z.; Huang, F.; Cao, Y.; Liang, Z.; Zhang, M.; Russell, T. P.; Chen, Y. Small-Molecule Solar Cells with Efficiency over 9%. *Nat. Photonics* **2015**, *9*, 35−41.
(45) Kan, B.; Zhang, Q.; Li, M.; Wan, X.; Ni, W.; Long, G.; Wang, Y.; Yang, X.; Feng, H.; Chen, Y. Solution-Processed Organic Solar Cells Based on Dialkylthiol-Substituted Benzodithiophene Unit with Efficiency near 10%. *J. Am. Chem. Soc.* **2014**, *136*, 15529−15532.
(46) Zhang, Y.; Kan, B.; Sun, Y.; Wang, Y.; Xia, R.; Ke, X.; Yi, Y. Q. Q.; Li, C.; Yip, H. L.; Wan, X.; Cao, Y.; Chen, Y. Nonfullerene Tandem Organic Solar Cells with High Performance of 14.11%. *Adv. Energy Mater.* **2018**, *30*, No. 1707508.
(47) Meng, L.; Yi, Y. Q. Q.; Wan, X.; Zhang, Y.; Ke, X.; Kan, B.; Wang, Y.; Xia, R.; Yip, H. L.; Li, C.; Chen, Y. A Tandem Organic Solar Cell with PCE of 14.52% Employing Subcells with the Same Polymer Donor and Two Absorption Complementary Acceptors. *Adv. Mater.* **2019**, *31*, No. 1804723.
(48) Zhang, X.; Ding, Y.; Feng, H.; Gao, H.; Ke, X.; Zhang, H.; Li, C.; Wan, X.; Chen, Y. Side Chain Engineering Investigation of Non-Fullerene Acceptors for Photovoltaic Device with Efficiency over 15%. *Sci. China Chem.* **2020**, *63*, 1799−1806.
(49) Wang, Y.; Zhang, Y.; Qiu, N.; Feng, H.; Gao, H.; Kan, B.; Ma, Y.; Li, C.; Wan, X.; Chen, Y. A Halogenation Strategy for over 12% Efficiency Nonfullerene Organic Solar Cells. *Adv. Energy Mater.* **2018**, *8*, No. 1702870.
(50) Zhang, Y.; Feng, H.; Meng, L.; Wang, Y.; Chang, M.; Li, S.; Guo, Z.; Li, C.; Zheng, N.; Xie, Z.; Wan, X.; Chen, Y. High Performance Thick-Film Nonfullerene Organic Solar Cells with Efficiency over 10% and Active Layer Thickness of 600 nm. *Adv. Energy Mater.* **2019**, *9*, No. 1902688.
(51) Ke, X.; Meng, L.; Wan, X.; Li, M.; Sun, Y.; Guo, Z.; Wu, S.; Zhang, H.; Li, C.; Chen, Y. The Rational and Effective Design of Nonfullerene Acceptors Guided by a Semi-Empirical Model for an Organic Solar Cell with an Efficiency over 15%. *J. Mater. Chem. A* **2020**, *8*, 9726−9732.
(52) Rau, U.; Blank, B.; Müller, T. C. M.; Kirchartz, T. Efficiency Potential of Photovoltaic Materials and Devices Unveiled by Detailed-Balance Analysis. *Phys. Rev. Appl.* **2017**, *7*, No. 044016.
(53) Röhr, J. A.; Moia, D.; Haque, S. A.; Kirchartz, T.; Nelson, J. Exploring the Validity and Limitations of the Mott-Gurney Law for Charge-Carrier Mobility Determination of Semiconducting Thin-Films. *J. Phys.: Condens. Matter* **2018**, *30*, No. 105901.
(54) Blom, P. W. M.; Mihailetchi, V. D.; Koster, L. J. A.; Markov, D. E. Device Physics of Polymer:Fullerene Bulk Heterojunction Solar Cells. *Adv. Mater.* **2007**, *19*, 1551−1566.
(55) Wu, J. L.; Chen, F. C.; Hsiao, Y. S.; Chien, F. C.; Chen, P.; Kuo, C. H.; Huang, M. H.; Hsu, C. S. Surface Plasmonic Effects of Metallic Nanoparticles on the Performance of Polymer Bulk Heterojunction Solar Cells. *ACS Nano* **2011**, *5*, 959−967.
(56) Hartnagel, P.; Kirchartz, T. Understanding the Light-Intensity Dependence of the Short-Circuit Current of Organic Solar Cells. *Adv. Theory Simul.* **2020**, *3*, No. 2000116.
(57) Baumann; Lorrmann; Rauh; Deibel; Dyakonov. A New Approach for Probing the Mobility and Lifetime of Photogenerated Charge Carriers in Organic Solar Cells Under Real Operating Conditions. *Adv. Mater.* **2012**, *24*, 4381−4386.
(58) Maurano, A.; Hamilton, R.; Shuttle, C. G.; Ballantyne, A. M.; Nelson, J.; O'Regan, B.; Zhang, W.; McCulloch, I.; Azimi, H.; Morana, M.; Brabec, C. J.; Durrant, J. R. Recombination Dynamics as a Key Determinant of Open Circuit Voltage in Organic Bulk Heterojunction Solar Cells: A Comparison of Four Different Donor Polymers. *Adv. Mater.* **2010**, *22*, 4987−4992.
(59) Shuttle, C. G.; O'Regan, B.; Ballantyne, A. M.; Nelson, J.; Bradley, D. D. C.; Durrant, J. R. Bimolecular Recombination Losses in Polythiophene: Fullerene Solar Cells. *Phys. Rev. B* **2008**, *78*, No. 113201.
(60) Wan, S.; Ma, Y.; Cai, D.; Lin, W.; Wang, P.; Wang, J.; Zheng, Q. Enhancing the Photovoltaic Performance of Ladder-Type Heteroheptacene-based Nonfullerene Acceptors by Incorporating Halogen Atoms on Their Ending Groups. *Adv. Funct. Mater.* **2021**, *31*, No. 2010436.
(61) Yunhao, C.; Yun, L.; Rui, W.; Hongbo, W.; Zhihao, C.; Jie, Z.; Zaifei, M.; Xiaotao, H.; Yong, Z.; Chunfeng, Z.; Fei, H.; Yanming, S. A Well-Mixed Phase Formed by Two Compatible Non-Fullerene Acceptors Enables Ternary Organic Solar Cells with Efficiency over 18.6%. *Adv. Mater.* **2021**, *33*, No. 2101733.
(62) Ge, J.; Hong, L.; Song, W.; Xie, L.; Zhang, J.; Chen, Z.; Yu, K.; Peng, R.; Zhang, X.; Ge, Z. Solvent Annealing Enables 15.39% Efficiency All-Small-Molecule Solar Cells through Improved Molecule Interconnection and Reduced Non-Radiative Loss. *Adv. Energy Mater.* **2021**, *11*, No. 2100800.
(63) Gao, S.; Bu, L.; Zheng, Z.; Wang, X.; Wang, W.; Zhou, L.; Hou, J.; Lu, G. Probing Film-Depth-Related Light Harvesting in Polymer Solar Cells via Plasma Etching. *AIP Adv.* **2017**, *7*, No. 045312.
(64) Wang, Z.; Hu, Y.; Xiao, T.; Zhu, Y.; Chen, X.; Bu, L.; Zhang, Y.; Wei, Z.; Xu, B. B.; Lu, G. Correlations between Performance of Organic Solar Cells and Film-Depth-Dependent Optical and Electronic Variations. *Adv. Opt. Mater.* **2019**, *7*, No. 1900152.
(65) Zhang, Y.; Deng, D.; Wang, Z.; Wang, Y.; Zhang, J.; Fang, J.; Yang, Y.; Lu, G.; Ma, W.; Wei, Z. Enhancing the Photovoltaic Performance via Vertical Phase Distribution Optimization in Small Molecule:PC71BM Blends. *Adv. Energy Mater.* **2017**, *7*, No. 1701548.
(66) Huo, Y.; Gong, X.-T.; Lau, T.-K.; Xiao, T.; Yan, C.; Lu, X.; Lu, G.; Zhan, X.; Zhang, H.-L. Dual-Accepting-Unit Design of Donor

https://doi.org/10.1021/acs.chemmater.1c04293
Chem. Mater. XXXX, XXX, XXX−XXX

Material for All-Small-Molecule Organic Solar Cells with Efficiency Approaching 11%. *Chem. Mater.* **2018**, *30*, 8661−8668.
(67) Wang, J.; Zhang, J.; Xiao, Y.; Xiao, T.; Zhu, R.; Yan, C.; Fu, Y.; Lu, G.; Lu, X.; Marder, S. R.; Zhan, X. Effect of Isomerization on High-Performance Nonfullerene Electron Acceptors. *J. Am. Chem. Soc.* **2018**, *140*, 9140−9147.

https://doi.org/10.1021/acs.chemmater.1c04293
Chem. Mater. XXXX, XXX, XXX−XXX